UC San Diego

UC San Diego Previously Published Works

Title

Chronic intermittent hypoxia attenuates noradrenergic innervation of hypoglossal motor nucleus

Permalink

https://escholarship.org/uc/item/4gz6n99r

Authors

Herlihy, Rachael

Frasson Dos Reis, Leonardo

Gvritishvili, Anzor

et al.

Publication Date

2024-03-01

DOI

10.1016/j.resp.2023.104206

Peer reviewed

eScholarship.org Powered by the California Digital Library
University of California

Author Manuscript

Author Manuscript

Author Manuscript

Author Manuscript

HHS Public Access

Author manuscript

Respir Physiol Neurobiol. Author manuscript; available in PMC 2024 September 01.

Published in final edited form as:

Respir Physiol Neurobiol. 2024 March ; 321: 104206. doi:10.1016/j.resp.2023.104206.

Chronic intermittent hypoxia attenuates noradrenergic innervation of hypoglossal motor nucleus

Rachael Herlihy[a], **Leonardo Frasson Dos Reis**[a], **Anzor Gvritishvili**[b], **Maya Kvizhinadze**[b], **Elizabeth Dybas**[a], **Atul Malhotra**[d], **Victor B. Fenik**[a,b,*], **Irma Rukhadze**[a,b,c,*]

[a]Department of Neuroscience and Experimental Therapeutics, Albany Medical College, Albany, NY 12208, USA

[b]VA West Los Angeles Medical Center, VAGLAHS, West Los Angeles, CA 90073, USA

[c]Department of Medicine, David Geffen School of Medicine at UCLA, Los Angeles, CA 90095, USA

[d]University of California San Diego, San Diego, CA 92093, USA

Abstract

The state-dependent noradrenergic activation of hypoglossal motoneurons plays an important role in the maintenance of upper airway patency and pathophysiology of obstructive sleep apnea (OSA). Chronic intermittent hypoxia (CIH), a major pathogenic factor of OSA, contributes to the risk for developing neurodegenerative disorders in OSA patients. Using anterograde tracer, channelrhodopsin-2, we mapped axonal projections from noradrenergic A7 and SubCoeruleus neurons to hypoglossal nucleus in DBH-cre mice and assessed the effect of CIH on these projections. We found that CIH significantly reduced the number of axonal projections from SubCoeruleus neurons to both dorsal (by 68%) and to ventral (by73%) subregions of the hypoglossal motor nucleus compared to sham-treated animals. The animals' body weight was also negatively affected by CIH. Both effects, the decrease in axonal projections and body weight, were more pronounced in male than female mice, which was likely caused by less sensitivity of female mice to CIH as compared to males. The A7 neurons appeared to have limited projections to the hypoglossal nucleus. Our findings suggest that CIH-induced reduction of noradrenergic innervation of hypoglossal motoneurons may exacerbate progression of OSA, especially in men.

*Correspondence to: Albany Medical College, 47 New Scotland Ave., MS-523B, Albany, NY 12208, USA. fenikv@amc.edu (V.B. Fenik), rukhadi@amc.edu (I. Rukhadze).

CRediT authorship contribution statement

Dybas Elizabeth: Data curation, Formal analysis, Visualization. **Malhotra Atul:** Writing – review & editing. **Fenik Victor B.:** Conceptualization, Data curation, Formal analysis, Funding acquisition, Investigation, Methodology, Project administration, Resources, Supervision, Validation, Visualization, Writing – original draft, Writing – review & editing. **Rukhadze Irma:** Conceptualization, Data curation, Formal analysis, Funding acquisition, Investigation, Methodology, Project administration, Resources, Supervision, Validation, Visualization, Writing – original draft, Writing – review & editing. **Herlihy Rachael:** Data curation, Formal analysis, Validation, Writing – original draft, Writing – review & editing, Visualization. **Dos Reis Leonardo Frasson:** Data curation, Formal analysis, Validation, Visualization. **Gvritishvili Anzor:** Data curation, Investigation, Methodology, Validation. **Kvizhinadze Maya:** Data curation, Investigation, Methodology, Visualization.

Conflict of interest

The authors have indicated no financial conflicts of interest.

Author Manuscript Author Manuscript Author Manuscript Author Manuscript

Keywords

Chronic intermittent hypoxia; Hypoglossal motoneurons; Obstructive sleep apnea; Noradrenergic neurons; Conditional anterograde tracers

1. Introduction

Obstructive sleep apnea (OSA) is a highly prevalent sleep-related breathing disorder characterized by repeated cycles of narrowing (hypopnea) or collapse (apnea) of upper airway during sleep (Jordan et al., 2014; Mezzanotte et al., 1992; Remmers et al., 1978; White, 2006). The prevalence of OSA increases with age and is 2–3 times higher in men than in women (Lin et al., 2008; Snyder and Cunningham, 2018; Won et al., 2020; Young et al., 1993). Recurrent apnea/hypopnea results in intermittent hypoxia and hypercapnia, and frequent arousals, all of which underlie OSA sequelae including neurocognitive and cardiometabolic effects (De Luca Canto et al., 2015; Dempsey et al., 2010; Djonlagic et al., 2012; Jordan et al., 2014; Ju et al., 2019; Kumar et al., 2014; Li and Veasey, 2012; Macey et al., 2013; Mokhlesi et al., 2016). The pathogenic factors of OSA may increase the risk of Alzheimer's disease and Parkinson's disease (Ju et al., 2019; Kaminska et al., 2022; Lajoie et al., 2020; Lal et al., 2022; Sun et al., 2020).

Hypoglossal motoneurons that innervate the genioglossus muscle, the main upper airway dilator, are critically involved in maintaining upper airway patency (Mezzanotte et al., 1992; Remmers et al., 1978). The upper airway muscle tone is elevated in patients with OSA during wakefulness, which is regarded as an adaptation to maintain the patency of anatomically compromised upper airway (Mezzanotte et al., 1992). However, the reduction of upper airway muscle tone during both rapid eye movement (REM) and non-REM (NREM) sleep counteracts with this adaptation and leads to decreased upper airway patency, a major neurological cause of OSA. The state-dependent decrease in activity of hypoglossal motoneurons is caused by two mechanisms: the withdrawal of noradrenergic excitation (Chan et al., 2006; Fenik et al., 2005) and the increase in cholinergic inhibition during REM sleep (Bellingham and Berger, 1996; Grace et al., 2013; Zhu et al., 2019). Neuroanatomical studies identified brainstem A7 and SubCoeruleus (SubC) neurons as major sources of noradrenergic innervation of hypoglossal motoneurons (Aldes et al., 1992; Rukhadze and Kubin, 2007), and it has been found that both A7 and SubC neurons become silent during REM sleep (Fenik and Rukhadze, 2022; Reiner, 1986; Rukhadze et al., 2008). Additionally, the excitatory functional coupling between A7 neurons and hypoglossal motoneurons has been demonstrated by clonidine-induced inhibition of A7 neurons (Fenik et al., 2008).

Chronic intermittent hypoxia (CIH), an animal model of OSA, has been shown to induce neurodegeneration and neuronal loss in the noradrenergic locus coeruleus, hippocampus, and several cortical regions (Gozal et al., 2001; Gozal et al., 2003; Sapin et al., 2015; Smith et al., 2013; Snyder et al., 2017; Xu et al., 2004; Zhu et al., 2007,). However, CIH has been found to increase the density of noradrenergic terminals of unknown origin in the ventromedial quadrant of the hypoglossal nucleus (Rukhadze et al., 2010). In this study, we hypothesized that CIH may differentially affect noradrenergic axonal projections

Author Manuscript Author Manuscript Author Manuscript Author Manuscript

to functionally different dorsal and ventral sub-regions of the hypoglossal nucleus, which innervate tongue retractors and protruders, respectfully.

To test this hypothesis, we took advantage of cell-type-specific approach of cre-dependent anterograde tracing and examined the impact of CIH on noradrenergic innervation of hypoglossal motoneurons originating from A7 and SubC noradrenergic neurons. We found that the ratio between the number of axonal projections, which were counted within both dorsal and ventral subdivisions of the hypoglossal nucleus, and SubC neurons that were transfected with AAV-ChR2 was decreased in mice exposed to CIH as compared to sham controls. This effect was more pronounced in male than female mice.

2. Materials and methods

2.1. Animals

The experiments were performed using 32 young (3–4 months old), 16 male and 16 female dopamine β-hydroxylase – cre (DBH-cre) mice (Tg(Dbh-cre)KH212Gsat/Mmucd or B6·FVB(Cg)-Tg(Dbh-cre) KH212Gsat/Mmucd). Hemizygous DBH-cre mice were purchased from the Mutant Mouse Regional Resource Center at the University of California, Davis, CA (stock # 032081 or 036778-UCD) and bred to C57BL6/J in our animal facility to produce offspring. DBH-cre mice were maintained on a C57BL6/J background and underwent genotyping using the tail DNA PCR analysis. This line of mouse was also used and validated in a prior experiment focused on the state-dependent activity of upper airway muscles during sleep and wakefulness (Rukhadze et al., 2017). Mice were housed with up to five individuals in one cage in an animal research facility of Veterans Administration of Greater Los Angeles Healthcare system (VAGLAHS), West Campus, on a 12:12-hr light-dark cycle with monitored temperature and humidity. Food and water were provided ad libitum. All experiments were approved and conducted in accordance with the guidelines of the Institutional Animal Care and Use Committee of the VAGLAHS and followed the National Institutes of Health Guide for the Care and Use of Laboratory Animals.

2.2. Conditional anterograde tracing

We used conditional anterograde tracing to map noradrenergic axonal projections from the brainstem A7 and SubC noradrenergic neurons to the hypoglossal motor nucleus in mice subjected to chronic intermittent hypoxia (CIH) or sham treatment. Unilateral injections of an adeno-associated viral vector (AAV8-Ef1a-DIO-hChR2(H134R)-mCherry, 1.7×10^{13} pfu/mL, (K. Diesseroth, UNC Vector Core, Chapel Hill, NC)) coding for Cre-dependent channelrhodopsin (ChR2) tagged with the red fluorescent protein mCherry were targeted at the A7 region in DBH-cre mice. In this AAV vector, the ChR2-mCherry sequence is inverted and surrounded by pairs of loxP and lox2272 sites, thus preventing nonspecific expression of ChR2-mCherry. By injecting this AAV-ChR2 (50–100 nl) in Cre-driver mice we achieved cell-type-specific transfection of noradrenergic neurons and their axonal projections (Geerling et al., 2017). All injections of AAV-ChR2 were made in pairs of male and female mice.

Author Manuscript Author Manuscript Author Manuscript Author Manuscript

For injections targeting the noradrenergic neurons in the A7 region, DBH-cre mice were anesthetized with an intraperitoneal (i.p.) injection of ketamine (100 mg/kg) and xylazine (10 mg/kg) in 0.9% saline, then placed into a stereotaxic apparatus (Model 940, David Kopf Instruments, Tujunga, CA). Unilateral injections of AAV-ChR2 were placed into the A7 region using the coordinates 1.5 mm lateral, 4.85 caudal to bregma, and 3.6 mm deep to dura. Microinjections were made using fine-tipped glass micropipettes (tip inner diameter 20–25 μm) by applying air pressure to the fluid in the pipette while monitoring the fluid meniscus movement in the pipette through a calibrated microscope to deliver AAV-ChR2 (50–100 nl). Each injection occurred over 3–5 min and was followed by a delay of 5 min before the pipette was slowly retracted. After removing the pipette from the injection site, the skin overlying the skull was closed with silk sutures and mice were then returned to their home cages and observed until full recovery. Postoperative care included twice-a-day observation of the animal's behavior and injections of analgesics (buprenorphine 0.5 mg/kg s.c. and meloxicam 5 mg/kg) to alleviate possible post-surgical discomfort.

2.3. Exposure to chronic intermittent hypoxia

After a week of recovery from surgical procedures mice were subjected to chronic intermittent hypoxia (CIH). Each pair of male and female mice that received AAV-ChR2 injection on the same day were divided into two groups: CIH (n = 16, 8 males and 8 females) or sham-treatment (n = 16, 8 males and 8 females). Throughout the experiment, the mice were housed, 5 per standard mouse cage, under 12/12 h light/dark cycle (light phase from 6:00 AM to 6:00 PM) with food and water provided ad libitum and cages changed after 5:00 PM every other day.

The mouse cages were placed inside custom-made chambers (height 22.9 cm, width 38.1 cm, depth 50.8 cm, and volume 44.3 L) in which level of oxygen (O2) was controlled by alternating flows of nitrogen (N2) and O2 (Oxycycler, Biospherix Ltd, Perish, NY). In CIH chambers, mice were exposed to cycling oxygen level with a 7 min period (10% O2 for 4 min and 21% O2 for 3 min) applied from 7:00 AM to 5:00 PM daily for 35 days. The flow of nitrogen (0.4 L/s for 50 s) decreased oxygen concentration to 10% in the CIH chamber whereas the flow of oxygen (0.4 L/s for 10 s) restored its concentration to 21%. The control mice were housed in identical chambers and experienced the sham air flow that mirrored gas exchanges in the CIH chambers (Fig. 1). The animals were individually weighed before entry into the study, after the first day of exposure, and then every day throughout the treatments. The duration of CIH exposure (35 days) used in this study was similar to CIH protocol that was sufficient to cause metabolic and neurological changes in our previous studies (Rukhadze et al., 2010; Stettner et al., 2012; Fenik et al., 2012).

2.4. Perfusions and tissue preparation

Animals were perfused at the end of CIH or sham treatment, which was the sixth week from AAV-ChR2 injections and is sufficient time for production and axon transport of AAV-ChR2 (Geerling et al., 2017). One day after the last day of CIH or sham exposure, the mice were pre-anesthetized with isoflurane (3%), deeply anesthetized with ketamine/xylazine (120/20 mg/kg I.P.) and perfused through the ascending aorta with phosphate-buffered saline (PBS, pH7.4, 100 mL) and heparin (1000 units/mL) at room temperature, followed by

Author Manuscript Author Manuscript Author Manuscript Author Manuscript

10% formalin in PBS (50 mL). Each brain was removed and postfixed overnight in 10% formalin-PBS at 4 °C. After cryoprotection in 30% sucrose-PBS, the brainstem was cut into 30-mm -thick coronal sections on a cryostat (CM1850, Leica), and the sections were collected in separate 1-in-3 series (90 mm between sections) of brainstem tissue sections. Sections were transferred to cryoprotectant solution and stored at − 20 °C until further processing.

2.5. Immunohistochemistry

To confirm that AAV-ChR2 was expressed only in noradrenergic neurons, we fluorescently double-labeled one series of brainstem sections from each mouse for DsRed (a marker for mCherry) and tyrosinehydroxylase (TH, a marker for catecholaminergic neurons). Our immunostaining procedures followed the basic protocol as described previously (Rukhadze et al., 2017). In brief, we removed a separate set of brainstem sections from each pair of mice from cryoprotectant and rinsed them in PBS. We double-labeled sections with a rabbit polyclonal antibody that binds DsRed-derived red-fluorescent proteins to enhance the native fluorescence of mCherry in AAV-ChR2-expressing neurons, and an anti-TH sheep polyclonal antibody to label noradrenergic and adrenergic neurons in the brainstem. Sections were washed in PBS and incubated overnight in primary DsRed antisera (1:1000, Clontech, cat. #632496, rabbit, polyclonal) and TH (1:1000, Millipore Sigma, cat. #AB1542 sheep polyclonal) diluted in PBS containing 0.25% Triton X-100 (PBST) for 24 h at room temperature. Sections were then washed in PBS and incubated in secondary antiserum Cy3-tagged anti-rabbit IgG (for DsRed; 1:500; Jackson ImmunoResearch Laboratories, Cat# 711–165–152); and Alexafluor488-tagged donkey anti-sheep antibody (for TH; 1:500; Invitrogen/Thermofisher, Cat# A11015) diluted in PBST for 2 h. To perform cell-type-specific axonal tracing from A7 and SubC noradrenergic neurons, we immunolabeled the second series of medullary sections from each mouse for DsRed (black) using nickel-enhanced 3,3′-diaminobenzidine hydrochloride (DAB). In brief, after washing sections in PBS, we incubated sections in 0.3% hydrogen peroxide prepared in PBS for 30 min to inactivate endogenous peroxidase. After additional PBS washes, we incubated sections overnight at room temperature in a primary antibody, rabbit anti-DsRed (which labels mCherry) (1:1000, Clontech, cat. #632496, polyclonal), prepared in PBST. The next day, we incubated sections for 2 h in biotinylated donkey anti-rabbit IgG secondary antiserum (1:500; Jackson ImmunoResearch 711–065–152) followed by 1 h in avidin–biotin complex (Vectastain ABC Elite Kit; Vector Laboratories, Burlingame, CA, Cat# PK-6100) and then labeled mCherry using DAB with hydrogen peroxide solution and ammonium nickel sulfate (DAB-kit, Vector Laboratories, Cat# SK-4100).

After fluorescent or DAB immunolabeling, we mounted and air-dried sections on Superfrost Plus slides (Fisher Scientific, Cat# 12–550–15). For sections with fluorescence immunolabeling, we coverslipped with Prolong Gold antifade mountant (Invitrogen #P36930) and stored in slide folders at 4°C until imaging. For DAB-labeled tissue, we counter-stained sections in neutral red for 10 min, dehydrated in graded ethanols for 1 min each and cleared in xylenes before coverslipping with a mounting media (Permaslip; Fisher Scientific, Cat# NC9183409).

Author Manuscript Author Manuscript Author Manuscript Author Manuscript

2.6. AAV-ChR2 injection site assessment and cell count

The noradrenergic neurons transfected with AAV-ChR2 in A7 and SubC regions were counted as DsRed-positive TH neurons in a series of sections with double fluorescence for TH and DsRed. Fluorescence whole-slide analyses were performed at 5x and 20x using a fluorescent microscope (Leica DML 2000). AAV-ChR2 tracer injection was targeted at the A7 nucleus in all mice. However, the injection sites were spread from the rostral end of the A7 nucleus up to the caudal end of the A5 nucleus in the ventrolateral pontine tegmentum. We excluded DBH-cre mice from data analysis, in which the transfection of the A5 or LC nuclei had been detected and analyzed the remaining DBH-cre mice (n = 19), in which the tracer injections resulted in the transfection of only A7 and/or SubC noradrenergic neurons. To assess the injection site and quantify the number of noradrenergic neurons transfected with AAV-ChR2, we counted DsRed-positive and TH-positive neurons in A7 and SubC regions using the fluorescently labeled brainstem sections (covering 5–14 (9.58 ± 0.66 (SE)) coronal pontine sections in each mouse). The neurons that were immunopositive for both TH and DsRed were considered as noradrenergic neurons “transfected” by the AAV-ChR2. Neuronal counts were performed from AP levels − 4.84 mm to − 5.52 mm from bregma according to the mouse brain atlas (Paxinos and Franklin, 2008).

2.7. Axon tracing and measurements

Axonal projections from ChR2-transfected A7 and SubC noradrenergic neurons were counted in hypoglossal motor nucleus using the DAB-stained medullary sections at the anteroposterior (AP) levels from − 8.0 mm to − 7.2 mm relative to bregma according to a mouse brain atlas (Paxinos and Franklin, 2008). The hypoglossal nucleus was outlined, and the individual axons identified within the hypoglossal nucleus were manually redrawn in entire cross-section of hypoglossal nucleus throughout the depth of each section (covering 9–15 (11.84 ± 0.29) coronal sections in each mouse). We performed axonal tracing using a 20x objective and upright microscope (Leica DML 2000) equipped with a tracing device (Leica L3/20). The tracing device allows an optical overlay of large objects (next to the microscope) on the microscope image, which made it possible to trace the outline of hypoglossal nucleus and each individual axon located within the nucleus. All axonal projections with DAB-immunolabeling for DsRed were redrawn bilaterally in the hypoglossal nucleus under direct microscopic observation that the focal plane could be changed and each individual axon would be traced throughout the dept of the section within the field of view. We did not reconstruct a 3D representation of these projections from individual neurons, but rather observed DAB-immunolabeled projections throughout the depth of each section.

For data analysis, the hypoglossal nucleus was divided into the dorsal and ventral subregions (Fig. 2). Axons were counted on final drawings for each section and separately analyzed for dorsal and ventral sub-regions, ipsi- and contra-laterally to the injection side in medullary sections from nine CIH and ten sham-treated mice. Axons that were in close proximity to each other were distinguished and counted separately. Axons that were fully contained within the hypoglossal nucleus were counted, whereas those that were outside or on the border of the hypoglossal nucleus without entering the nucleus were not counted. No noradrenergic boutons were counted. If an axon crossed a border between subregions of the

Author Manuscript Author Manuscript Author Manuscript Author Manuscript

hypoglossal nucleus, this axon was counted only for one subregion. Axons that bifurcated within a focal plane were counted as two axons. In two animals included in data analysis, where axonal projections could not be quantified due to artifacts with DAB immunostaining, we used medullary sections with immunofluorescence labeling for DsRed. The individuals blinded to the treatment groups have performed axonal tracing and counting.

2.8. Statistical analysis

We used two-tailed Student's t-test, one-way analysis of variance, and linear regression analyses for normally distributed data; for not normally distributed data, the Wilcoxon signed rank and Mann-Whitney rank sum tests were used (Sigma Plot, ver. 13.0, Systat Software, Inc., San Jose, CA; GraphPad Software, Prism 10.0.2, Boston, MA). Differences were considered significant when $p < 0.05$. The variability of means was described by the standard error (SE) throughout the report.

3. Results

3.1. Distribution of noradrenergic neurons transfected with AAV-ChR2

As confirmed by immunohistochemical assessment, the tracer injection sites were spread rostro-caudally from the rostral end of the A7 nucleus down to the caudal end of the A5 nucleus in the ventrolateral pontine tegmentum. The specificity of the neuronal transfection was verified by the lack of detectable cellular or axonal immunostaining in brain sections from the 3 littermate mice that received the same AAV-ChR2 injections as DBH-cre mice. We analyzed *only* the DBH-cre mice (n = 19), in which the tracer injections resulted in the transfection of noradrenergic neurons in A7 and/or SubC nuclei and excluded DBH-cre mice from data analysis, in which substantial transfection of the A5 or LC nuclei had been detected (Fig. 3). In these 19 mice, the number of ChR2-positive A7 noradrenergic neurons ranged from 0 to 51 (mean: 20.8 ± 3.4) and the number of ChR2-positive SubC noradrenergic neurons, from 0 to 93 (mean: 40.6 ± 7.1), due to inevitable discrepancies between locations of tracer injection sites and A7/SubC nuclei in each mouse. In all mice included in data analysis, the transfection of NA neurons was observed in either A7 (n = 1), SubC (n = 2) or both (n = 16). Quantitative analysis of ChR2 expression in noradrenergic neurons revealed that 94.1% of A7 and 95.0% of SubC neurons that expressed ChR2 were also immunolabeled for TH, which was similar to the expression of a cre-dependent gene in A7 and SubC neurons of DBH-cre mice in our previous study (Rukhadze et al., 2017).

3.2. Effect of CIH on animal's body weight

From the 19 mice included in the analysis, 9 mice were exposed to CIH (5 males and 4 females) and 10 mice were sham-treated (5 males and 5 females). The body weight was significantly higher in male as compared to female mice before the start of CIH/sham treatment (day 0) (24.7 g + 0.62, n = 10, vs. 19.8 g + 0.42, n = 9, $p < 0.001$, t-test). All animals gained weight during the 35 days of CIH/sham treatment (sham males: from 24.8 g + 1.0 to 29.3 g + 0.74, n = 5, $p < 0.01$; CIH males: from 24.7 g + 0.83 to 28.0 g + 1.2, n = 5, $p < 0.01$; sham females: from 19.7 g + 0.70 to 22.3 g + 0.49, n = 5, $p < 0.01$; and CIH females: from 20.0 g + 0.45 to 22.3 g + 0.64, n = 4, $p < 0.01$; paired t-tests) (Fig. 4). However, in male mice, there was a tendency of a drop in body weight on day 1 of the CIH

Author Manuscript Author Manuscript Author Manuscript Author Manuscript

exposure, which resulted in their body weight staying significantly lower than sham controls for the duration of the remaining 34 days of treatment (Fig. 4, two top traces, $p < 0.001$, one-way ANCOVA, equal slopes model), which was similar to the reduced body weight of male rats during CIH exposure previous study (Rukhadze et al., 2010). Contrary, there was no CIH effect on the body weights in female mice relative to sham treatment (Fig. 4, two bottom traces, $p = 0.7$, one-way ANCOVA, equal slopes model).

3.3. Afferent noradrenergic axonal projections within the hypoglossal motor nucleus

The cell-type-specific transfection of A7/SubC noradrenergic neurons in the 19 DBH-cre mice resulted in the selective anterograde labeling of their axon projections within the hypoglossal motor nucleus (Fig. 5). To evaluate the neurochemical specificity of axons projecting to the hypoglossal nucleus, we verified the presence of ChR2 in axons immunolabeled for TH confirming the selective tracing of axonal projections derived from ChR2-transfected neurons in A7 and SubC regions (Fig. 5D).

The ChR2-expressing axons originating from A7 and SubC neurons were counted within the hypoglossal nucleus in medullary sections that were immunolabeled for DsRed with DAB (9–15 coronal sections per mouse covering the rostro-caudal extent of hypoglossal nucleus) (Fig. 6).

The total number of noradrenergic axonal projections counted within the hypoglossal nucleus in each animal ranged from 45 to 2078 (mean: 1043 ± 229) in the 9 CIH-treated mice and from 86 to 1930 (mean: 907 ± 171) in the 10 sham-treated mice.

The noradrenergic axonal projections were similarly distributed between ipsi- and contra-lateral sides of the hypoglossal nucleus, both dorsally and ventrally (Fig. 7). However, there were significantly more axonal counts in the dorsal subregion of the hypoglossal nucleus as compared to the ventral subregion ipsi- (36.1 ± 7.6 vs. 20.3 ± 4.7, $p < 0.01$, n = 10; paired t-test) and contra-laterally (31.7 ± 6.4 vs. 18.0 ± 3.7, $p < 0.01$, n = 10; paired t-test) (Fig. 7). There was no significant effect of CIH on the noradrenergic axon count at either dorsal or ventral parts of the hypoglossal nucleus (t-test).

To assess the rostro-caudal distribution of the axonal projections within the hypoglossal nucleus, we grouped sections from the rostral (AP levels [− 7.2; −7.32]), central [− 7.48; −7.64], and caudal [− 7.76; − 8.00] parts of the hypoglossal nucleus, in which the axons were quantified (Fig. 8). The ChR2-positive axonal projections were similarly distributed along the rostro-caudal extent of the hypoglossal motor nucleus in both the dorsal and ventral subregions (Fig. 8). The mean axon counts in the dorsal and ventral subregions of the hypoglossal nucleus were respectively 53.3 ± 10.5 and 24.0 ± 5.1 for the rostral part; 59.3 ± 11.4 and 30.1 ± 7.1 for the central part; and 51.2 ± 8.2 and 31.0 ± 6.0 for the caudal part.

3.4. Relationship between the number of transfected noradrenergic neurons in A7 and SubC nuclei and their axonal projections to the hypoglossal nucleus

Since there were no statistically significant differences between ipsiand contra-lateral sides and between the rostro-caudal regions of the hypoglossal nucleus, we grouped these data together for further analyses. The multiple linear regression analysis revealed that the

Author Manuscript Author Manuscript Author Manuscript Author Manuscript

number of ChR2-transfected SubC neurons significantly ($p < 0.001$) predicted the axon count within the hypoglossal nucleus in the 10 sham-treated mice (Fig. 9A), whereas there was no significant relationship between the axon count and the number of ChR2-transfected A7 neurons ($p = 0.53$, Fig. 9B). In addition, the simple linear regression analysis of the axon-neuron relationships showed a strong regression coefficient for the SubC neurons ($R^2 = 0.94$) and a weak coefficient for the ChR2-transfected A7 neurons ($R^2 = 0.083$) (Fig. 9).

3.5. Effect of CIH on the axon-neuron relationship originating from A7 and SubC nuclei

We assessed the effect of CIH on the number of noradrenergic axonal projections separately to the dorsal and ventral subregions of the hypoglossal nucleus, in which functionally different hypoglossal motoneurons are located (Aldes, 1995; Dobbins and Feldman, 1995). The CIH treatment reduced the slope of the axon-neuron relationships for the transfected SubC neurons at both dorsal and ventral parts of the hypoglossal nucleus (Fig. 10A, C), whereas no effect of CIH was observed for the transfected A7 neurons (Fig. 10B, D). The slope of liner regression was reduced from 1.4 axon/neuron in sham-treated mice ($R^2 = 0.94$, $p < 0.0001$, n = 10) to 0.93 axon/neuron in the CIH-treated mice ($R^2 = 0.60$, $p < 0.05$, n = 9) within the dorsal part of the hypoglossal nucleus (Fig. 10A). Similarly, the exposure to CIH decreased the slope of the regression in the ventral region from 0.83 axon/neuron ($R^2 = 0.91$, $p < 0.0001$, n = 10) to 0.49 axon/neuron ($R^2 = 0.46$, $p < 0.05$, n = 9) (Fig. 10C). Since these data passed the internal equal slope test in the ANCOVA, we could not use this analysis to test whether the effect of CIH on the regression slopes was significant, although the ANCOVA detected significant ($p < 0.05$) difference between the regressions for sham- and CIH-treated mice using the equal slope model for both dorsal and ventral hypoglossal regions.

3.6. Effect of CIH on the ratio between noradrenergic axon count within the hypoglossal nucleus and the number of transfected SubC neurons

The linear regression analysis showed that the axon count within both dorsal and ventral regions significantly depended on the number of transfected SubC neurons, but not the A7 neurons, in both sham- and CIH-treated mice. This result suggests that most of the axons that were counted in the hypoglossal nucleus originated from the SubC nucleus. Therefore, we used the ratio between the noradrenergic axon counts and the number of transfected SubC neurons (AC/N) that were counted in each animal within dorsal and ventral subdivisions of the hypoglossal nucleus to assess the effect of CIH on these projections. Fig. 11 shows that CIH exposure similarly reduces the AC/N ratio in dorsal and ventral parts of the hypoglossal nucleus by 68% and 73%, respectively. The AC/N ratio was significantly reduced in CIH- (n = 8, one animal was excluded due to the lack of ChR2 expression in SubC cells) compared to sham-treated mice (n = 10) in dorsal (1.08 axon/neuron ± 0.17 vs. 3.38 axon/neuron ± 1.1, $p < 0.01$, Mann-Whitney test) and ventral (0.532 axon/neuron ± 0.12 vs. 1.99 axon/neuron ± 0.69, $p < 0.01$, Mann-Whitney test) subdivisions of the hypoglossal motor nucleus (Fig. 11).

To assess the effect of CIH on the number of A7 and SubC noradrenergic axonal projections to the hypoglossal nucleus, we used both the linear regression analysis (Fig. 10), and the ratio of noradrenergic axon count within the hypoglossal nucleus to the number of

Author Manuscript Author Manuscript Author Manuscript Author Manuscript

transfected SubC neurons (Fig. 11). The slope “k” in the regression equation “AC=k * N + b” (Fig. 10) and the ratio “r” (r = AC/N) (Fig. 11) have similar meanings: they both estimate the number of axons that are produced by one neuron (A – number of axon count, N – number of neurons). However, the regression approach produces consistently smaller numbers for the slope “k” as compared to the ratio “r” due to the inherent difference in their calculations. The regression slope yields more precise estimation of the slope “k” due to excluding “other” axons, which are represented by the constant “b” in the regression equation. This is more evident when the regression formula is transformed as k = (AC-b)/N, as opposed to the ratio r = AC/N.

3.7. Effect of CIH on the axon count-neuron ratio (AC/N) for SubC neurons in male and female mice

To assess the sex difference in the CIH effect, we combined the axon counts in the dorsal and ventral hypoglossal regions so that the AC/N ratio represented the ratio between the total axon count within the hypoglossal nucleus and the number of transfected SubC neurons in each animal. We found that in sham-treated mice, SubC tended to have more projections to hypoglossal motor nucleus in male (AC/N = 7.53 axon/neuron + 3.5, n = 4), as compared to female mice (AC/N = 3.22 axon/neuron + 0.43, n = 5; $p = 0.55$, Mann-Whitney test) (Fig. 12).

Following CIH exposure, the AC/N ratio was significantly reduced in male mice (from 7.53 axon/neuron ± 3.5, n = 4, in sham group; to 1.37 axon/neuron ± 0.32, n = 4, in CIH group; $p < 0.05$, Mann-Whitney test). In female mice, the depressant effect of CIH on the AC/N ratio did not reach the significance level (3.22 axon/neuron ± 0.43, n = 5, in sham group vs. 1.85 axon/neuron ± 0.48, n = 5, in CIH group; $p = 0.2$, Mann-Whitney test). The relative effect of CIH on the AC/N ratio tended to be higher in male mice (82%) as compared to female mice (42%) (Fig. 12).

4. Discussion

The main finding of the present neuroanatomical study is that exposure to CIH decreases noradrenergic axonal projections from SubC neurons to motoneurons in both dorsal and ventral subregions of the hypoglossal nucleus, and this effect is more prevalent in male than female mice. Also, the CIH-induced loss of body weight was substantially greater in male as compared to female mice. We used the linear regression analysis to estimate the average contribution of transfected noradrenergic neurons located in A7 and SubC nuclei to the observed innervation of the hypoglossal nucleus. Our findings suggests that SubC noradrenergic neurons provide direct innervation of the hypoglossal motoneurons whereas noradrenergic input from A7 neurons appeared to be limited.

4.1. The impact of CIH on innervation of hypoglossal motoneurons by SubC neurons

In this study, we achieved cell-type-specific transfections of A7 and SubC cells and quantified their axonal projections to the hypoglossal motor nucleus. We assessed both the strength of hypoglossal innervation that originates from each of the nuclei and the effect of CIH on these projections using the linear regression analysis between ChR2-transfected

Author Manuscript Author Manuscript Author Manuscript Author Manuscript

noradrenergic neurons and ChR2-positive axons counted within the hypoglossal nucleus. We found a significant correlation between axon counts within the hypoglossal subregions and transfected noradrenergic neurons for SubC, but not for A7 nuclei. This finding suggests that SubC neurons provide direct innervation to hypoglossal motoneurons, while A7 neurons may innervate the hypoglossal nucleus through indirect pathways. The prior reports utilized conventional retrograde tracers, which were lacking genetic specificity (Aldes et al., 1992; Rukhadze and Kubin, 2007) and could spread to the adjacent regions outside the hypoglossal nucleus thereby labeling fibers of passage (Bruinstroop et al., 2012). This was always regarded as a limitation for the identification of specific noradrenergic inputs to hypoglossal motoneurons (Aldes et al., 1992; Rukhadze and Kubin, 2007). Conversely, we employed conditional anterograde tracing to map A7 and SubC projections, in a cell-type-specific manner, to functionally distinct hypoglossal motoneurons.

Based on the distribution of hypoglossal motoneurons that innervate different muscles of the tongue, the hypoglossal nucleus has been divided into two functionally different dorsal (innervates tongue retractors) and ventral (innervates tongue protruders) subregions (Altschuler et al., 1994; Aldes, 1995; Dobbins and Feldman, 1995; Fay and Norgren, 1997; Rukhadze et al., 2010; Kubin, 2016). The present study assessed for the first time the number and distribution pattern of noradrenergic axonal projections to hypoglossal motoneurons innervating these functionally different upper airway muscles that are crucial for upper airway patency (Aldes, 1995; Dobbins and Feldman, 1995; El-Chami et al., 2017; Mateika et al., 1999; Mezzanotte et al., 1992; Oliven et al., 2007).

We used linear regression to separate projections between two distinct groups of transfected neurons to their targets and report the even distribution of SubC noradrenergic projections throughout the entire rostral-caudal extent of the hypoglossal nucleus in both dorsal and ventral subregions. The finding that A7 neurons may affect hypoglossal motoneurons using indirect projections is in agreement with the hypothesis that state-dependent noradrenergic control of hypoglossal motoneuron activity is mainly carried out by A7 neurons, and this control is not direct but rather mediated by interneurons located in the pre-hypoglossal medullary region (Fenik, 2015; Frasson et al., 2023; Rukhadze and Fenik, 2016).

It was previously reported that, in rats, CIH increased the number of noradrenergic terminals of unknown origin in a part of ventromedial quadrant of the hypoglossal nucleus, where motoneurons retrogradely labelled from the base of the tongue were found (Rukhadze et al., 2010). However, the number of noradrenergic terminals closely opposed to the retrogradely labeled motoneurons were not altered by CIH exposure (Rukhadze et al., 2010). In the present study using the cell-type-specific labeling in mice, we determined that SubC projections in both the dorsal and ventral subregions throughout the rostro-caudal extent of the hypoglossal nucleus were decreased in CIH-treated mice as compared to the sham-treated group. Therefore, catecholaminergic neurons, other than SubC, may be responsible for the CIH-induced increase of terminals in the previous study.

Our finding that the exposure to CIH decreases noradrenergic innervation of the hypoglossal nucleus originating from SubC cells suggests a decrease of the excitatory noradrenergic drive to hypoglossal motoneurons in animals exposed to CIH. This would in part

Author Manuscript Author Manuscript Author Manuscript Author Manuscript

counteract with previously found increase of sensitivity of hypoglossal motoneurons to α1-adrenoreceptor agonists in rats that were exposed to a similar protocol of CIH treatment (Stettner et al., 2012). In addition, the CIH-induced decrease of the noradrenergic drive to hypoglossal motoneurons would also hinder to a degree the previously found increase in the tonus of the genioglossus muscle in OSA patients (Mezzanotte et al., 1992). Therefore, the SubC noradrenergic neurons may not be the ones that contribute to the hypothesized CIH- and OSA-induced activation of the genioglossus muscle during wakefulness (Mezzanotte et al., 1992; Rukhadze et al., 2010).

CIH exposure causes oxidative stress, an increase in blood pressure, and an array of metabolic effects, which might also be experienced by OSA patients (Dempsey et al., 2010; Khalyfa et al., 2021; Fenik et al., 2012; Conde et al., 2023). One of earlier studies (Dematteis et al., 2008) observed hemodynamic alterations including elevated blood pressure (predominantly diastolic) and brady-tachyarrhythmia in male mice after 14 days of CIH exposure. While the present study did not directly assess the effect of CIH on hemodynamics and metabolism, we believe that these adverse effects that were elicited by CIH may contribute to the decrease of noradrenergic innervation of the hypoglossal nucleus.

The CIH approach simulates only intermittent hypoxia that is experienced by OSA patients but not hypercapnia, which is commonly associated with partial or complete obstruction of upper airway in OSA patients. Indeed, in our previous CIH experiments, the increase in respiratory frequency during oxygen level nadir (10%) could be seen by visual assessment in rats, which could induce hypocapnia (unpublished observations). However, the increase in systemic levels of norepinephrine and angiotensin in CIH-exposed rats was found to be not affected by the presence or absence of hypercapnia, which suggest that changes in CO2 level are not detrimental factor in CIH exposure (reviewed in Fletcher, 2001). Conversely, oxidative stress caused by CIH has been identified as a major detrimental factor of CIH and OSA (Xu et al., 2004; Zhu et al., 2007; Dempsey et al., 2010; Li and Veasey, 2012). In addition, respiratory effects in mice that were induced by CIH exposure in present study were minimal by visual inspection, which suggested negligible changes in systemic CO_2 level during CIH in mice as compared to rats.

The much smaller effect of CIH on both the body weight and on noradrenergic SubC projections to the hypoglossal nucleus that was observed in this study could be explained by less sensitivity of female mice to CIH due to antioxidant property of estrogen (Huang et al., 2018). In addition, female rats showed higher ventilatory response to sustained hypoxia at high altitude compared to males (Joseph et al., 2000). The better ventilatory response to CIH would reduce the hypoxia level that is experienced by female mice during CIH exposure in our experiments, which would further reduce sensitivity of female mice to harmful effect of CIH.

4.2. Contribution of CIH-related decrease of noradrenergic innervation to the sleep-related depression of hypoglossal motoneurons

The sleep-related hypotonia of upper airway muscles is the major neurological cause of OSA, which is characterized by recurrent episodes of upper airway narrowing or obstruction during sleep in those who are anatomically predisposed (Jordan et al., 2014; Mezzanotte

Author Manuscript Author Manuscript Author Manuscript Author Manuscript

et al., 1992; Remmers et al., 1978; White, 2006). Functionally, the activity of hypoglossal motoneurons is depressed during REM sleep by two mechanisms of approximately equal strength: withdrawal of noradrenergic excitation to hypoglossal motoneurons (Chan et al., 2006; Fenik et al., 2005; Fenik, 2015) and increased cholinergic inhibition of hypoglossal motoneurons (Bellingham and Berger, 1996; Grace et al., 2013; Zhu et al., 2019). The withdrawal mechanism is also supported by the findings that SubC and A7 noradrenergic neurons are silent during REM sleep (Fenik and Rukhadze, 2022; Reiner, 1986; Rukhadze et al., 2008). Our finding that SubC neurons project to the hypoglossal nucleus bilaterally and in a uniform manner suggests that these noradrenergic neurons may co-activate both protruder and retractor tongue muscles. While the activation of the genioglossus muscle, which is innervated primarily by ventral hypoglossal motoneurons, has been associated with pharyngeal airway enlargement during the awake state, a co-activation of the tongue retractor muscles, which are innervated by dorsal hypoglossal motoneurons, may be necessary to fully maintain upper airway patency (Aldes, 1995; Dobbins and Feldman, 1995; El-Chami et al., 2017; Mateika et al., 1999; Mezzanotte et al., 1992; Oliven et al., 2007). Altogether, our findings suggest that the CIH-induced reduction of noradrenergic co-activation of both tongue protruder and retractor muscles originating from SubC cells may exacerbate the severity of OSA.

4.3. Functional implications

In individuals with OSA, frequent apnea/hypopnea results in intermittent hypoxemia, which affects neurocognition, the cardiovascular system, and metabolism (De Luca Canto et al., 2015; Dempsey et al., 2010; Djonlagic et al., 2012; Jordan et al., 2014; Ju et al., 2019; Kumar et al., 2014; Li and Veasey, 2012; Macey et al., 2013; Mokhlesi et al., 2016), and ultimately may increase the risk of developing Alzheimer's disease and Parkinson's disease (Ju et al., 2019; Kaminska et al., 2022; Kumar et al., 2014; Lajoie et al., 2020; Lal et al., 2022; Sun et al., 2020).

Our neuroanatomical findings suggest that CIH induces a degeneration of excitatory noradrenergic projections from SubC cells to upper airway motoneurons. This effect may exacerbate severity and contribute to progression of OSA. Therefore, the protection of SubC noradrenergic neurons and their axons could serve as a potential novel therapeutic target for OSA treatment. In summary, our finding that the suppressant effect of CIH on noradrenergic innervation of hypoglossal motoneurons was more prominent in male than female mice may explain the neuronal mechanism of increased prevalence of OSA in men (Lin et al., 2008; Snyder and Cunningham, 2018; Won et al., 2020; Young et al., 1993).

Acknowledgements

This study was supported by NIH Grants NHLBI R01HL133847 (to IR and VBF) and NIA R01AG065233 (to IR and VBF). We thank Dr. Jerome M. Siegel for donating the BioSpherix OxyCycler system.

Data Availability

Data will be made available on request.

Author Manuscript Author Manuscript Author Manuscript Author Manuscript

References

Aldes LD, 1995. Subcompartmental organization of the ventral (protrusor) compartment in the hypoglossal nucleus of the rat. J. Comp. Neurol 3531, 89–108.

Aldes LD, Chapman ME, Chronister RB, Haycock JW, 1992. Sources of noradrenergic afferents to the hypoglossal nucleus in the rat. Brain Res. Bull 296, 931–942.

Altschuler SM, Bao X, Miselis RR, 1994. Dendritic architecture of hypoglossal motoneurons projecting to extrinsic tongue musculature in the rat. J. Comp. Neurol 3424, 538–550.

Bellingham MC, Berger AJ, 1996. Presynaptic depression of excitatory synaptic inputs to rat hypoglossal motoneurons by muscarinic m2 receptors. J. Neurophysiol 766, 3758–3770.

Bruinstroop E, Cano G, Vanderhorst VG, Cavalcante JC, Wirth J, Sena-Esteves M, Saper CB, 2012. Spinal projections of the a5, a6 (locus coeruleus), and a7 noradrenergic cell groups in rats. J. Comp. Neurol 5209, 1985–2001.

Chan E, Steenland HW, Liu H, Horner RL, 2006. Endogenous excitatory drive modulating respiratory muscle activity across sleep-wake states. Am. J. Respir. Crit. Care Med 17411, 1264–1273.

Conde SV, Polotsky VY, Joseph V, Kinkead R, 2023. On the origins of sleep disordered breathing, cardiorespiratory and metabolic dysfunction: which came first, the chicken or the egg? J. Physiol

De Luca Canto G, Pachêco-Pereira C, Aydinoz S, Major PW, Flores-Mir C, Gozal D, 2015. Biomarkers associated with obstructive sleep apnea and morbidities: a scoping review. Sleep. Med 163, 347–357.

Dematteis M, Julien C, Guillermet C, Sturm N, Lantuejoul S, Mallaret M, Lévy P, Gozal E, 2008. Intermittent hypoxia induces early functional cardiovascular remodeling in mice. Am. J. Respir. Crit. Care Med 1772, 227–235.

Dempsey JA, Veasey SC, Morgan BJ, O'Donnell CP, 2010. Pathophysiology of sleep apnea. Physiol. Rev 901, 47–112.

Djonlagic I, Saboisky J, Carusona A, Stickgold R, Malhotra A, 2012. Increased sleep fragmentation leads to impaired off-line consolidation of motor memories in humans. PLoS One 73, e34106.

Dobbins EG, Feldman JL, 1995. Differential innervation of protruder and retractor muscles of the tongue in rat. J. Comp. Neurol 3573, 376–394.

El-Chami M, Sudan S, Lin HS, Mateika JH, 2017. Exposure to intermittent hypoxia and sustained hypercapnia reduces therapeutic cpap in participants with obstructive sleep apnea. J. Appl. Physiol 1234, 993–1002.

Fay RA, Norgren R, 1997. Identification of rat brainstem multisynaptic connections to the oral motor nuclei using pseudorabies virus. Iii. Lingual muscle motor systems. Brain Res. Brain Res. Rev 253, 291–311.

Fenik VB, 2015. Revisiting antagonist effects in hypoglossal nucleus: Brainstem circuit for the state-dependent control of hypoglossal motoneurons: a hypothesis. Front Neurol. 6, 254. [PubMed: 26648908]

Fenik VB, Rukhadze I, 2022. Activity of pontine a7 noradrenergic neurons is suppressed during rem sleep. J. Appl. Physiol (1985) 1331, 130–143.

Fenik VB, Davies RO, Kubin L, 2005. Rem sleep-like atonia of hypoglossal (xii) motoneurons is caused by loss of noradrenergic and serotonergic inputs. Am. J. Respir. Crit. Care Med 17210, 1322–1330.

Fenik VB, Rukhadze I, Kubin L, 2008. Inhibition of pontine noradrenergic a7 cells reduces hypoglossal nerve activity in rats. Neuroscience 1572, 473–482.

Fenik VB, Singletary T, Branconi JL, Davies RO, Kubin L, 2012. Glucoregulatory consequences and cardiorespiratory parameters in rats exposed to chronic-intermittent hypoxia: effects of the duration of exposure and losartan. Front Neurol. 3, 51. [PubMed: 22509173]

Fletcher EC, 2001. Invited review: physiological consequences of intermittent hypoxia: systemic blood pressure. J. Appl. Physiol (1985) 904, 1600–1605.

Frasson LR, Xu K, Rukhadze I, Fenik VB, 2023. Genioglossus muscle (gg) activity evoked by pharmacological stimulation of alpha1-adrenoceptors in pre-hypoglossal region (phr). Sleep 46 (Suppl), 0038.

Author Manuscript Author Manuscript Author Manuscript Author Manuscript

Geerling JC, Yokota S, Rukhadze I, Roe D, Chamberlin NL, 2017. Kölliker-fuse gabaergic and glutamatergic neurons project to distinct targets. J. Comp. Neurol 5258, 1844–1860.

Gozal D, Daniel JM, Dohanich GP, 2001. Behavioral and anatomical correlates of chronic episodic hypoxia during sleep in the rat. J. Neurosci 217, 2442–2450.

Gozal D, Row BW, Kheirandish L, Liu R, Guo SZ, Qiang F, Brittian KR, 2003. Increased susceptibility to intermittent hypoxia in aging rats: Changes in proteasomal activity, neuronal apoptosis and spatial function. J. Neurochem 866, 1545–1552.

Grace KP, Hughes SW, Horner RL, 2013. Identification of the mechanism mediating genioglossus muscle suppression in rem sleep. Am. J. Respir. Crit. Care Med 1873, 311–319.

Huang YC, Yuan ZF, Yang CH, Shen YJ, Lin JY, Lai CJ, 2018. Estrogen modulates the sensitivity of lung vagal C fibers in female rats exposed to intermittent hypoxia. Front Physiol. 9, 847. [PubMed: 30026705]

Jordan AS, McSharry DG, Malhotra A, 2014. Adult obstructive sleep apnoea. Lancet 3839918, 736–747.

Joseph V, Soliz J, Pequignot J, Semporé B, Cottet-Emard JM, Dalmaz Y, Favier R, Spielvogel H, Pequignot JM, 2000. Gender differentiation of the chemoreflex during growth at high altitude: functional and neurochemical studies. Am. J. Physiol. Regul. Integr. Comp. Physiol 278, R806–R816. [PubMed: 10749766]

Ju YS, Zangrilli MA, Finn MB, Fagan AM, Holtzman DM, 2019. Obstructive sleep apnea treatment, slow wave activity, and amyloid-β. Ann. Neurol 852, 291–295.

Kaminska M, O'Sullivan M, Mery VP, Lafontaine AL, Robinson A, Gros P, Martin JG, Benedetti A, Kimoff RJ, 2022. Inflammatory markers and bdnf in obstructive sleep apnea (osa) in parkinson's disease (pd). Sleep. Med 90, 258–261. [PubMed: 35228136]

Khalyfa A, Ericsson A, Qiao Z, Almendros I, Farré R, Gozal D, 2021. Circulating exosomes and gut microbiome induced insulin resistance in mice exposed to intermittent hypoxia: effects of physical activity. EBioMedicine 64, 103208. [PubMed: 33485839]

Kubin L, 2016. Neural control of the upper airway: respiratory and state-dependent mechanisms. Compr. Physiol 64, 1801–1850.

Kumar R, Pham TT, Macey PM, Woo MA, Yan-Go FL, Harper RM, 2014. Abnormal myelin and axonal integrity in recently diagnosed patients with obstructive sleep apnea. Sleep 374, 723–732.

Lajoie AC, Lafontaine AL, Kimoff RJ, Kaminska M, 2020. Obstructive sleep apnea in neurodegenerative disorders: current evidence in support of benefit from sleep apnea treatment. J. Clin. Med 92.

Lal C, Ayappa I, Ayas N, Beaudin AE, Hoyos C, Kushida CA, Kaminska M, Mullins A, Naismith SL, Osorio RS, Phillips CL, Parekh A, Stone KL, Turner AD, Varga AW, 2022. The link between obstructive sleep apnea and neurocognitive impairment: an official american thoracic society workshop report. Ann. Am. Thorac. Soc 198, 1245–1256.

Li Y, Veasey SC, 2012. Neurobiology and neuropathophysiology of obstructive sleep apnea. Neuromolecular Med 143, 168–179.

Lin CM, Davidson TM, Ancoli-Israel S, 2008. Gender differences in obstructive sleep apnea and treatment implications. Sleep. Med Rev 126, 481–496.

Macey PM, Kumar R, Woo MA, Yan-Go FL, Harper RM, 2013. Heart rate responses to autonomic challenges in obstructive sleep apnea. PLoS One 810, e76631.

Mateika JH, Millrood DL, Kim J, Rodriguez HP, Samara GJ, 1999. Response of human tongue protrudor and retractors to hypoxia and hypercapnia. Am. J. Respir. Crit. Care Med 1606, 1976–1982.

Mezzanotte WS, Tangel DJ, White DP, 1992. Waking genioglossal electromyogram in sleep apnea patients versus normal controls (a neuromuscular compensatory mechanism). J. Clin. Invest 895, 1571–1579.

Mokhlesi B, Ham SA, Gozal D, 2016. The effect of sex and age on the comorbidity burden of osa: an observational analysis from a large nationwide us health claims database. Eur. Respir. J 474, 1162–1169.

Author Manuscript Author Manuscript Author Manuscript Author Manuscript

Oliven A, Odeh M, Geitini L, Oliven R, Steinfeld U, Schwartz AR, Tov N, 2007. Effect of coactivation of tongue protrusor and retractor muscles on pharyngeal lumen and airflow in sleep apnea patients. J. Appl. Physiol (1985) 1035, 1662–1668.

Paxinos G, Franklin KBJ, 2008. The mouse brain in stereotaxic coordinates. Academic Press, New York.

Reiner PB, 1986. Correlational analysis of central noradrenergic neuronal activity and sympathetic tone in behaving cats. Brain Res 3781, 86–96.

Remmers JE, deGroot WJ, Sauerland EK, Anch AM, 1978. Pathogenesis of upper airway occlusion during sleep. J. Appl. Physiol. Respir. Environ. Exerc Physiol 446, 931–938.

Rukhadze I, Fenik VB, 2016. Control of hypoglossal motoneuron excitability by noradrenergic neurons is not direct. Sleep 39 (Suppl), 0127.

Rukhadze I, Kubin L, 2007. Differential pontomedullary catecholaminergic projections to hypoglossal motor nucleus and viscerosensory nucleus of the solitary tract. J. Chem. Neuroanat 331, 23–33.

Rukhadze I, Fenik VB, Branconi JL, Kubin L, 2008. Fos expression in pontomedullary catecholaminergic cells following rapid eye movement sleep-like episodes elicited by pontine carbachol in urethane-anesthetized rats. Neuroscience 1521, 208–222.

Rukhadze I, Fenik VB, Benincasa KE, Price A, Kubin L, 2010. Chronic intermittent hypoxia alters density of aminergic terminals and receptors in the hypoglossal motor nucleus. Am. J. Respir. Crit. Care Med 18210, 1321–1329.

Rukhadze I, Carballo NJ, Bandaru SS, Malhotra A, Fuller PM, Fenik VB, 2017. Catecholaminergic a1/c1 neurons contribute to the maintenance of upper airway muscle tone but may not participate in nrem sleep-related depression of these muscles. Respir. Physiol. Neurobiol 244, 41–50. [PubMed: 28711601]

Sapin E, Peyron C, Roche F, Gay N, Carcenac C, Savasta M, Levy P, Dematteis M, 2015. Chronic intermittent hypoxia induces chronic low-grade neuroinflammation in the dorsal hippocampus of mice. Sleep 3810, 1537–1546.

Smith SM, Friedle SA, Watters JJ, 2013. Chronic intermittent hypoxia exerts cns region-specific effects on rat microglial inflammatory and tlr4 gene expression. PLoS One 812, e81584.

Snyder B, Cunningham RL, 2018. Sex differences in sleep apnea and comorbid neurodegenerative diseases. Steroids 133, 28–33. [PubMed: 29258810]

Snyder B, Shell B, Cunningham JT, Cunningham RL, 2017. Chronic intermittent hypoxia induces oxidative stress and inflammation in brain regions associated with early-stage neurodegeneration. Physiol. Rep 59.

Stettner GM, Fenik VB, Kubin L, 2012. Effect of chronic intermittent hypoxia on noradrenergic activation of hypoglossal motoneurons. J. Appl. Physiol (1985) 1122, 305–312.

Sun AP, Liu N, Zhang YS, Zhao HY, Liu XL, 2020. The relationship between obstructive sleep apnea and parkinson's disease: a systematic review and meta-analysis. Neurol. Sci 415, 1153–1162.

White DP, 2006. The pathogenesis of obstructive sleep apnea: advances in the past 100 years. Am. J. Respir. Cell Mol. Biol 341, 1–6.

Won CHJ, Reid M, Sofer T, Azarbarzin A, Purcell S, White D, Wellman A, Sands S, Redline S, 2020. Sex differences in obstructive sleep apnea phenotypes, the multi-ethnic study of atherosclerosis. Sleep 435.

Xu W, Chi L, Row BW, Xu R, Ke Y, Xu B, Luo C, Kheirandish L, Gozal D, Liu R, 2004. Increased oxidative stress is associated with chronic intermittent hypoxia-mediated brain cortical neuronal cell apoptosis in a mouse model of sleep apnea. Neuroscience 1262, 313–323.

Young T, Palta M, Dempsey J, Skatrud J, Weber S, Badr S, 1993. The occurrence of sleep-disordered breathing among middle-aged adults. N. Engl. J. Med 32817, 1230–1235.

Zhu L, Chamberlin NL, Arrigoni E, 2019. Muscarinic inhibition of hypoglossal motoneurons: possible implications for upper airway muscle hypotonia during rem sleep. J. Neurosci 3940, 7910–7919.

Zhu Y, Fenik P, Zhan G, Mazza E, Kelz M, Aston-Jones G, Veasey SC, 2007. Selective loss of catecholaminergic wake active neurons in a murine sleep apnea model. J. Neurosci 2737, 10060–10071.

Author Manuscript Author Manuscript Author Manuscript Author Manuscript

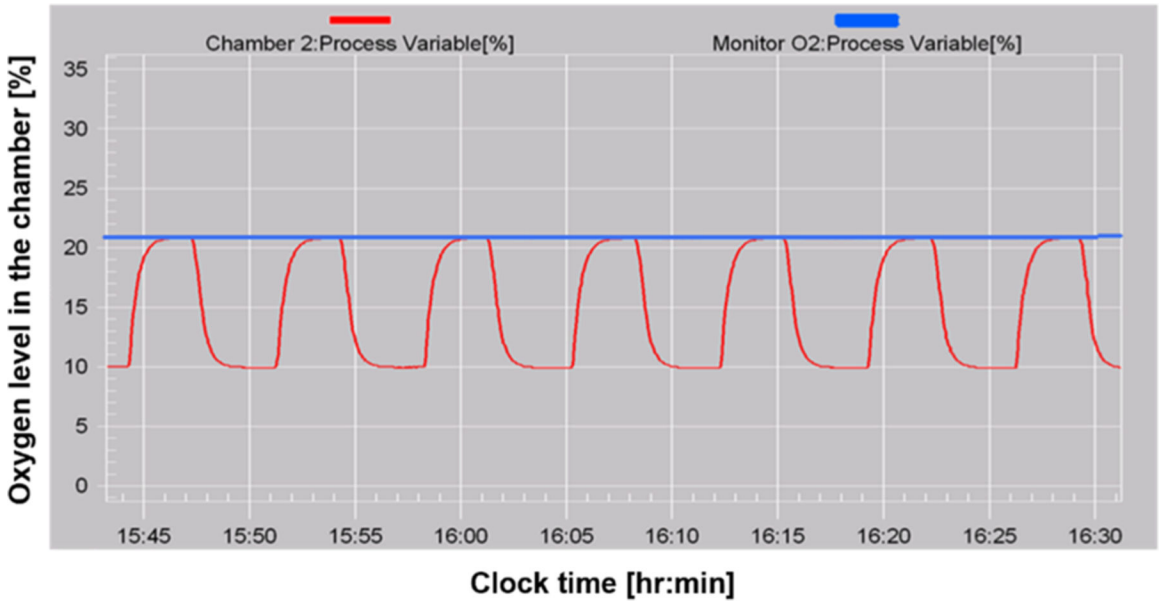

Fig. 1.

Time course of oxygen levels in chambers with intermittent hypoxia (Chamber 2, red line) and sham (Monitor O2, blue line) treatments.

Author Manuscript Author Manuscript Author Manuscript Author Manuscript

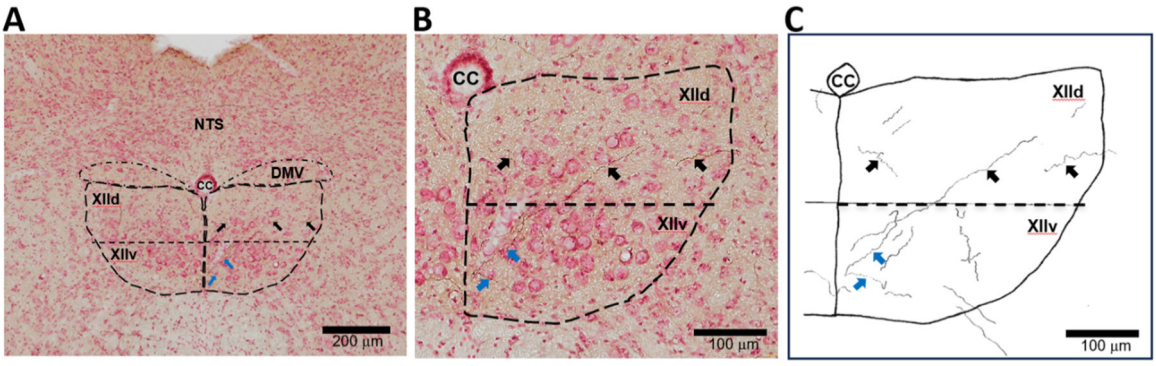

Fig. 2. Representative example of redrawn noradrenergic axonal projections to the hypoglossal motor nucleus in a sham-treated male mouse (case AG57).

A: Low magnification image of a medullary coronal section at the caudal region of the hypoglossal nucleus that corresponds to AP − 7.92 mm relative to bregma. **B:** High magnification image of the right side of the hypoglossal nucleus (shown on panel **A**). **C:** Example of redrawn DsRed-positive noradrenergic axonal projections (black fibers) that were found within the right part hypoglossal nucleus (shown in panel **B**) under direct microscopic observation throughout the depth of the section (x20 objective). The borders of the hypoglossal and dorsal vagal motor nuclei are shown by curved dashed lines, while the division between dorsal and ventral subregions are shown by a straight dashed line. Black and blue arrows point to examples of well visible axonal projections in the dorsal and ventral subregions of the hypoglossal nucleus, respectively. Abbreviations: cc - central canal; DMV - dorsal motor nucleus of vagus; NTS - nucleus of the solitary tract; XIId - dorsal subregion of hypoglossal nucleus; XIIv - ventral subregion of hypoglossal nucleus.

Author Manuscript Author Manuscript Author Manuscript Author Manuscript

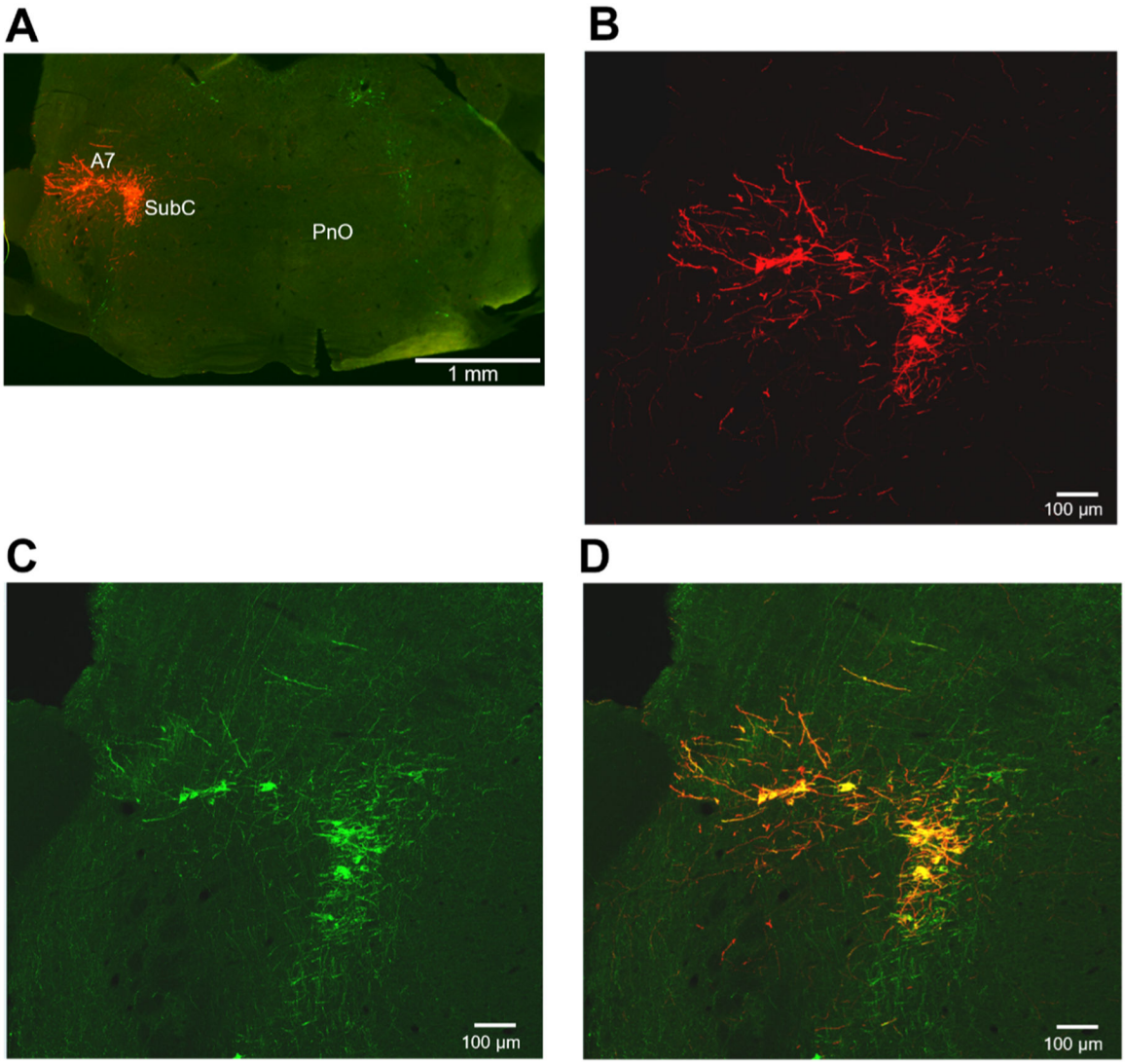

Fig. 3. The majority of ChR2-transfected A7 and SubC neurons were noradrenergic.

A: The low magnification confocal image demonstrates double-labeled neurons in A7 and SubC regions in a sham-treated female mouse (case AG42) at AP − 4.96 mm. **B-D:** The high magnification confocal images of these transfected noradrenergic neurons show ChR2-positive (red) neurons (**B**), TH-positive (green) noradrenergic neurons (**C**), and double-labeled (orange) neurons (**D**). Quantitative analysis revealed that 94.1% of A7 and 95.0% of SubC neurons that expressed ChR2 were also immunolabeled for TH. Abbreviations: PnO – pontine reticular nucleus, oral part.

Author Manuscript Author Manuscript Author Manuscript Author Manuscript

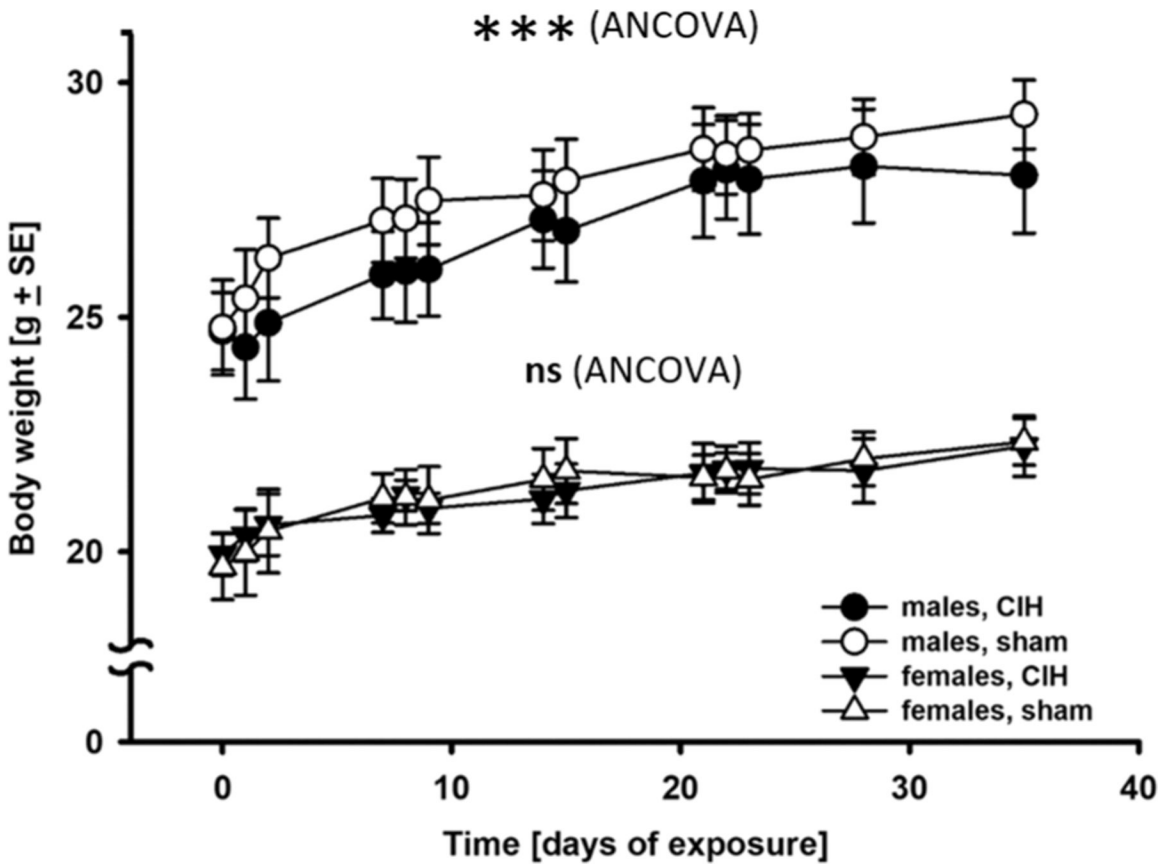

Fig. 4. CIH reduced body weight in male mice.

Before CIH/sham treatment (day 0), body weight was significantly higher in males as compared with females (24.7 g + 0.62, n = 10, vs. 19.8 g + 0.42, n = 9, $p < 0.001$, t-test). However, body weight of male mice decreased on day 1 of CIH exposure. This decrease was not statistically significant, but it affected the body weight in the males during the CIH exposure. The body weight of both males and females gradually increased during CIH, however, it remained significantly lower compared with sham controls in males (*** $p <$ 0.001, one-way ANCOVA, equal slopes model), but not in the female group.

Author Manuscript Author Manuscript Author Manuscript Author Manuscript

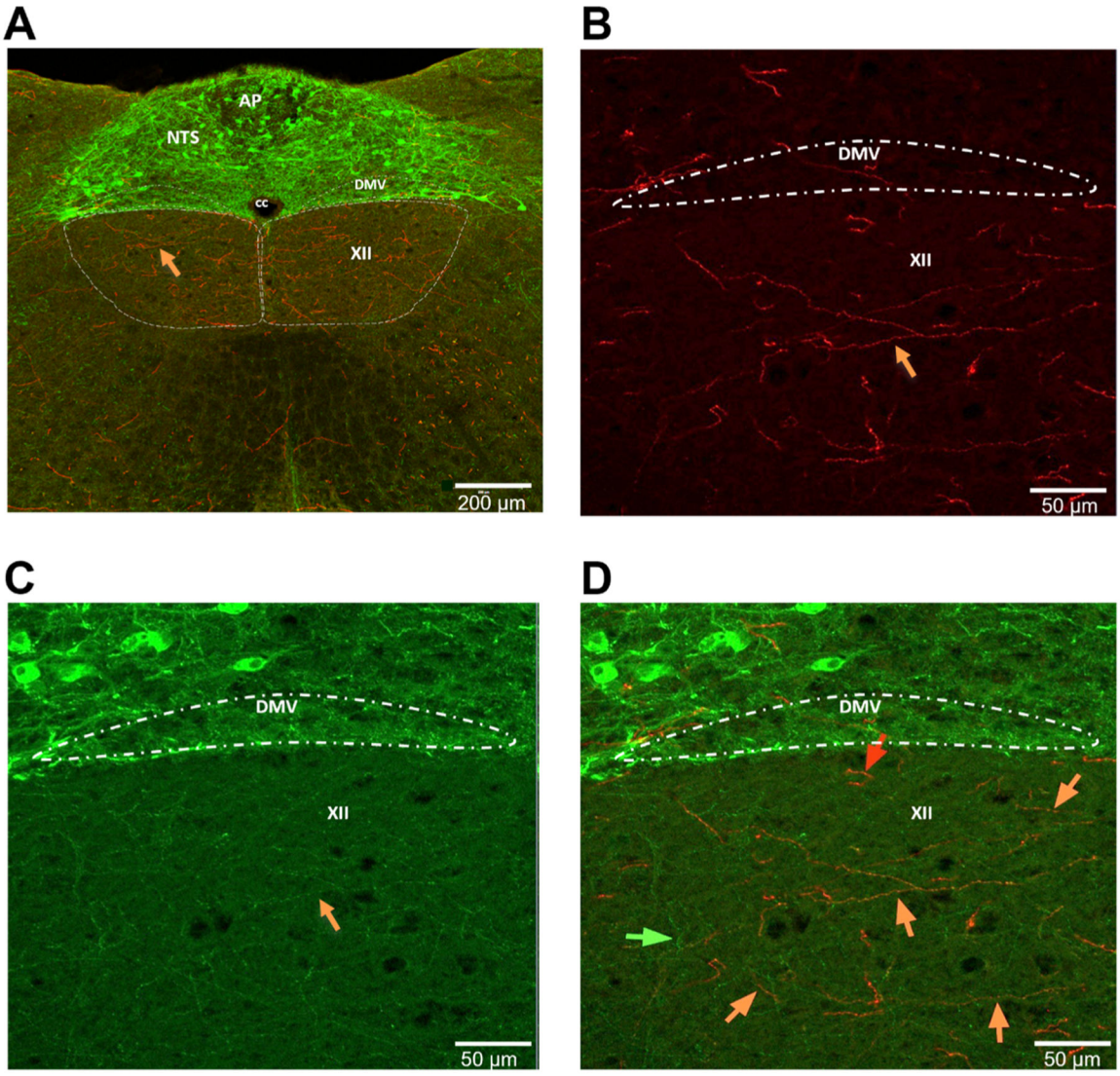

Fig. 5. Most noradrenergic projections originating from A7 and SubC nuclei expressed ChR2.

A: Low magnification confocal image demonstrates double-labeled projections in hypoglossal nucleus originating from A7 and SubC neurons in a sham-treated female mouse (case AG49) at AP − 7.56 mm. **B–D:** High magnification confocal images of projections from transfected noradrenergic neurons show ChR2-positive (red) axons (**B**), TH-positive (green) axons (**C**), and double-labeled (orange) axons (**D**). The orange arrows point to the double-labeled noradrenergic axons. The red arrow shows a ChR2-positive fiber that is TH-negative, and the green arrow points to the TH-positive axon, which does not express ChR2. Abbreviations: DMV – dorsal motor nucleus of vagus; cc – central canal; AP – area postrema; NTS – nucleus of the solitary tract; XII – hypoglossal motor nucleus.

Author Manuscript Author Manuscript Author Manuscript Author Manuscript

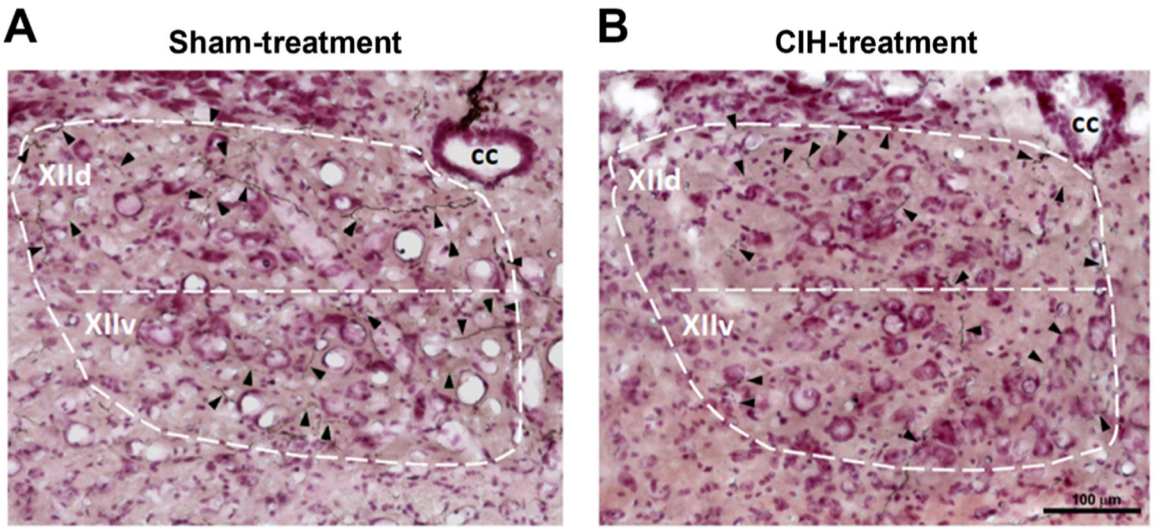

Fig. 6. DAB-stained, ChR2-positive axonal projections were more numerous in the dorsal than ventral subregion of the hypoglossal nucleus.

A, B: Noradrenergic projections (black arrows) in hypoglossal nucleus that originated from A7 and SubC nuclei are shown in a pair of brain sections matched for AP level taken from sham- (**A,** case AG33) and CIH-treated (**B,** case AG31) male mice that received unilateral injections of AAV-ChR2. Abbreviations: XIId – dorsal subregion of hypoglossal nucleus; XIIv – ventral subregion of hypoglossal nucleus; cc – central canal.

Author Manuscript Author Manuscript Author Manuscript Author Manuscript

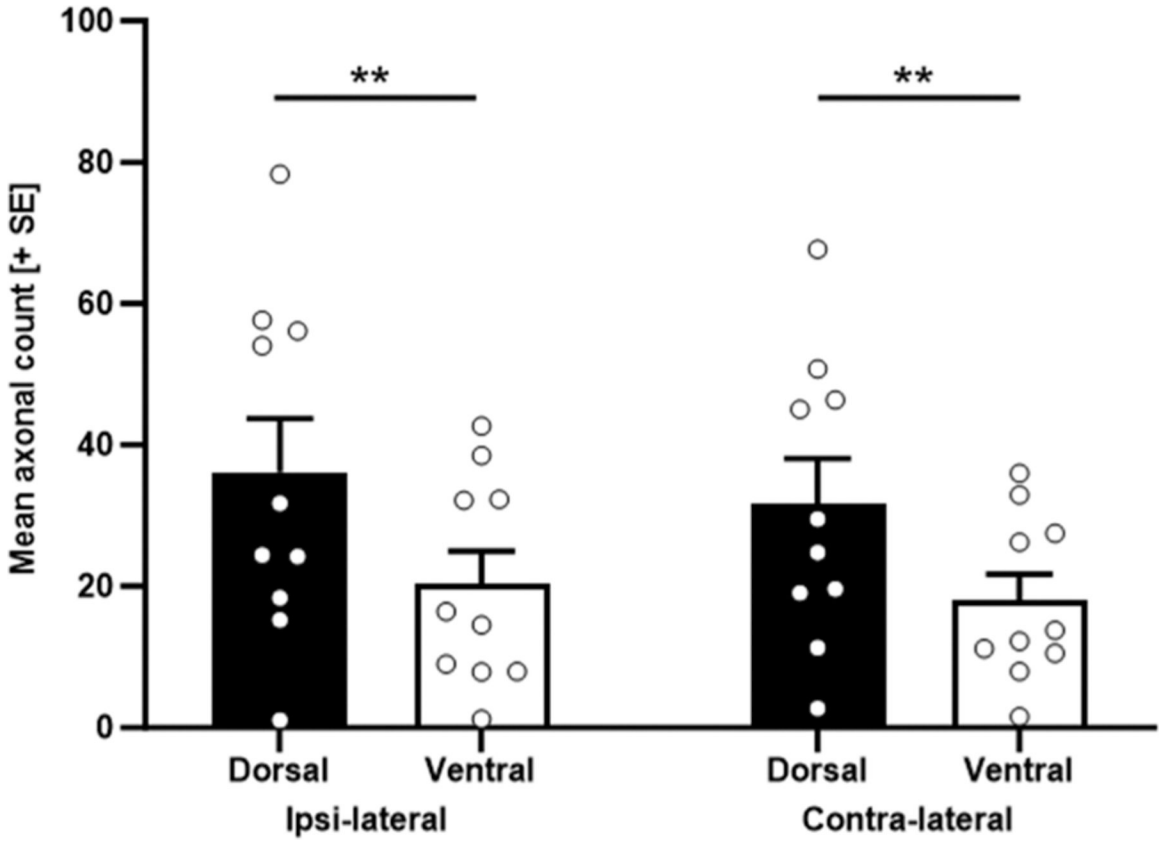

Fig. 7. Noradrenergic axonal counts were higher in the dorsal vs. the ventral subregions of the hypoglossal nucleus, but they were similar at ipsi- and contra-lateral sides of the hypoglossal nucleus.

Prevalence of noradrenergic projections that originated from A7 and SubC nuclei were greater in the dorsal than ventral subregion of the hypoglossal nucleus, on both the ipsiand contra-lateral sides in male and female sham-treated mice (n = 10). Abbreviations: * * - $p <$ 0.01.

Author Manuscript Author Manuscript Author Manuscript Author Manuscript

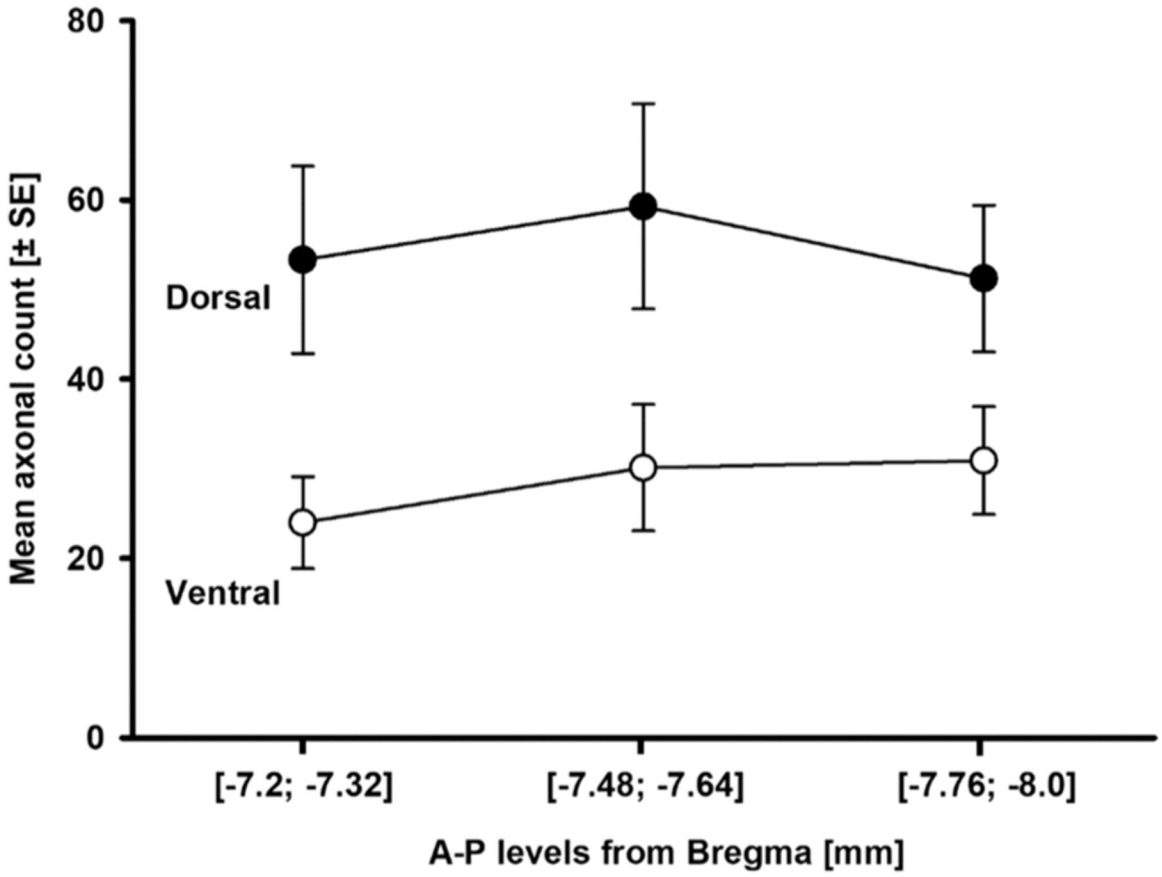

Fig. 8. Noradrenergic projections that originated from A7 and SubC nuclei were similarly distributed throughout the rostro-caudal extent of the hypoglossal nucleus.

This distribution was similar across rostral (AP levels [−7.2; −7.32]), central (AP levels [−7.48; −7.64]), and caudal (AP levels [−7.76; −8.00]) regions of the hypoglossal motor nucleus, both in dorsal and ventral subregions of the hypoglossal nucleus, in male and female sham-treated mice (n = 10).

Author Manuscript Author Manuscript Author Manuscript Author Manuscript

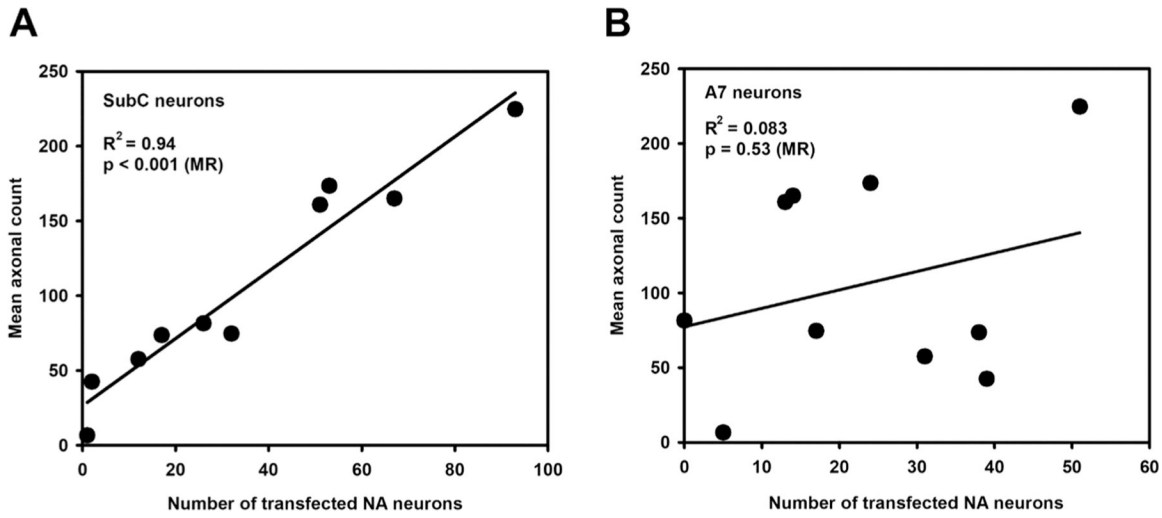

Fig. 9. The number of SubC neurons transfected with AAV-ChR2 strongly predicted the number of noradrenergic axonal projections to the hypoglossal nucleus.

A: The noradrenergic axon counts within the hypoglossal nucleus significantly correlated with the number of SubC neurons transfected with AAV-ChR2 in sham-treated animal (male and female) group ($p < 0.001$, multiple linear regression; $R^2 = 0.94$, simple linear regression; n = 10). B: However, the correlation with transfected A7 neurons was not significant (p = 0.53, multiple linear regression; $R^2 = 0.083$, simple linear regression; n = 10). Abbreviations: NA – noradrenergic; MR – multiple linear regression.

Author Manuscript Author Manuscript Author Manuscript Author Manuscript

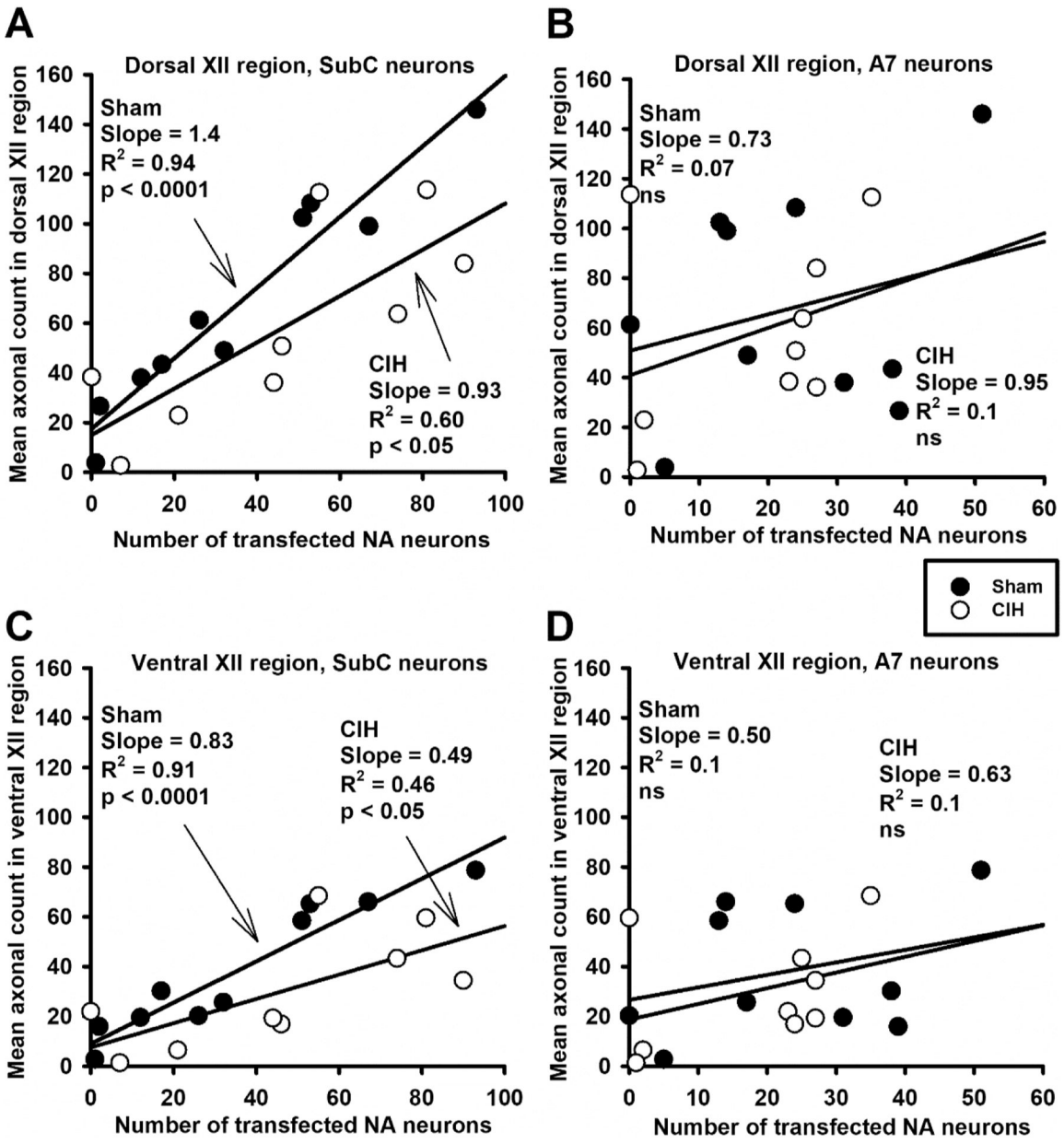

Fig. 10. CIH exposure reduces the slope of the axon-neuron relationships for transfected SubC neurons within both dorsal and ventral subregions of the hypoglossal nucleus, but not for A7 neurons.

A: The slope of liner regression was reduced from 1.4 axon/neuron in sham-treated male and female mice ($R^2 = 0.94$, $p < 0.0001$, n = 10) to 0.93 axon/neuron in the CIH-treated male and female mice ($R^2 = 0.60$, $p < 0.05$, n = 9) at the dorsal part of the hypoglossal nucleus. C: In the ventral region, the exposure to CIH decreased the slope of the regression from 0.83 axon/neuron ($R^2 = 0.91$, $p < 0.0001$, n = 10) to 0.49 axon/neuron ($R^2 = 0.46$, $p < 0.05$, n = 9). B, D: There were no significant correlations for transfected A7 neurons in either the dorsal (B) or ventral (D) subregions in sham- or CIH-treated groups. Abbreviations: ns - not significant, XII – hypoglossal motor nucleus.

Author Manuscript Author Manuscript Author Manuscript Author Manuscript

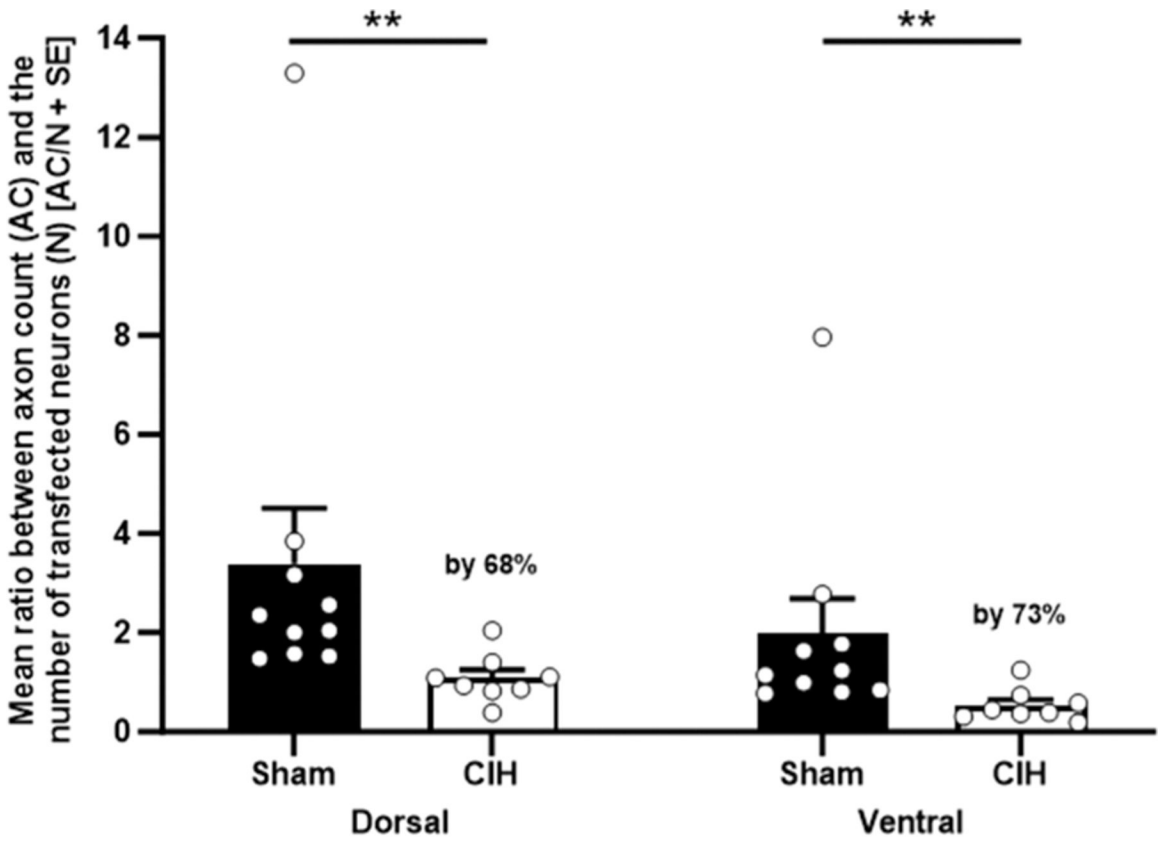

Fig. 11. CIH reduced the ratio between the axon count within the hypoglossal nucleus and the number of transfected noradrenergic SubC neurons (AC/N).

The AC/N ratio was significantly reduced in CIH- (male and female mice, n = 8, one animal was excluded due to the lack of ChR2 expression in SubC cells) compared to sham-treated male and female mice (n = 10) in dorsal (1.08 axon/neuron ± 0.17 vs. 3.38 axon/neuron ± 1.1, $p < 0.01$, Mann-Whitney test) and ventral subdivisions (0.532 axon/neuron ± 0.12 vs. 1.99 axon/neuron ± 0.69, $p < 0.01$, Mann-Whitney test) of the hypoglossal motor nucleus. The reduction of the AC/N ratio was similar in dorsal and ventral parts of the hypoglossal nucleus by 68% and 73%, respectively. Abbreviations: * * - $p < 0.01$.

Author Manuscript Author Manuscript Author Manuscript Author Manuscript

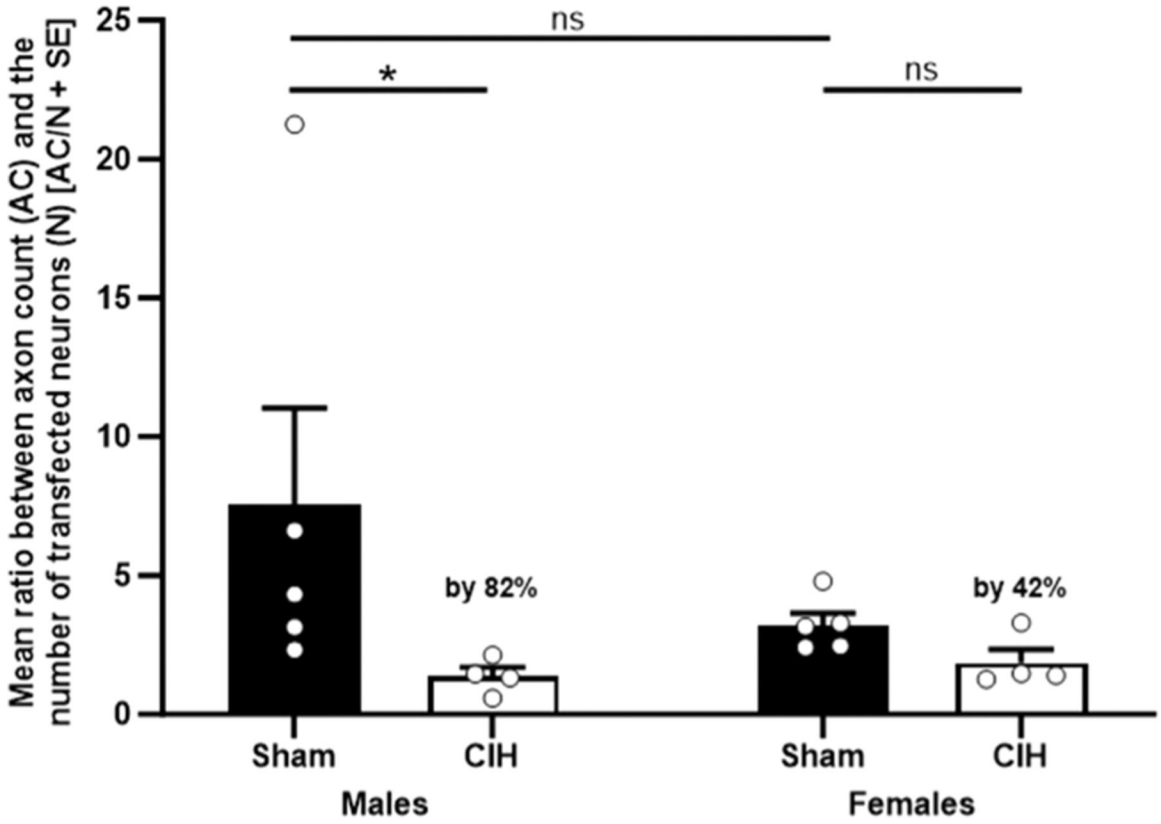

Fig. 12. CIH reduced SubC projections to the hypoglossal nucleus more prominently in male than female mice.

In male mice, CIH significantly reduced the AC/N ratio from 7.53 axon/neuron ± 3.5 (n = 4, sham group) to 1.37 axon/neuron ± 0.32 (n = 4, CIH group, $p < 0.05$). The depressant effect of CIH on the AC/N ratio did not reach the significance level in female mice (3.22 axon/neuron ± 0.43, n = 5, in sham group vs. 1.85 axon/neuron ± 0.48, n = 5, in CIH group; $p = 0.2$; Mann-Whitney tests). The relative effect of CIH on the AC/N ratio tended to be higher in male mice (82%) as compared to female mice (42%). Abbreviations: * - $p < 0.05$; ns - not significant.